INTERNATIONAL JOURNAL FOR NUMERICAL METHODS IN FLUIDS
Int. J. Numer. Meth. Fluids 2005; **48**:631–648
Published online 7 March 2005 in Wiley InterScience (www.interscience.wiley.com). DOI: 10.1002/fld.943

Fringe element reconstruction for front tracking for three-dimensional incompressible flow analysis

Du-Soon Choi[1], Seung-Seob Lee[2,‡] and Yong-Taek Im[1,*,†]

[1]*Computer Aided Materials Processing Laboratory, Department of Mechanical Engineering, ME3227, Korea Advanced Institute of Science and Technology, 373-1 Gusongdong, Yusonggu, Taejon 305-701, South Korea*
[2]*Micro Mechanical System Technology Laboratory, Department of Mechanical Engineering, Korea Advanced Institute of Science and Technology, 373-1 Gusongdong, Yusonggu, Taejon 305-701, South Korea*

SUMMARY

Fringe element reconstruction technique for tracking the free surface in three-dimensional incompressible flow analysis was developed. The flow field was calculated by the mixed formulation based on a four-node tetrahedral element with a bubble function at the centroid (P1+/P1). Since an Eulerian approach was employed in this study, the flow front interface was advected by the flow through a fixed mesh. For accurate modelling of interfacial movement, a fringe element reconstruction method developed can provide not only an accurate treatment of material discontinuity but also surface tension across the interface. The effect of surface tension was modelled by imposing tensile stress directly on the constructed surface elements at the flow front interface. To verify the numerical approach developed, the developed algorithm was applied to two examples whose solutions are available in references. Good agreement was obtained between the simulation results and these solutions. Copyright © 2005 John Wiley & Sons, Ltd.

KEY WORDS: three-dimensional flow; free surface; front tracking; finite element method; fringe element reconstruction

INTRODUCTION

Free surface flows and interfaces between two immiscible fluids or materials with different phases are observed in many natural and industrial processes. Especially at the filling stages of mould flow, the accurate prediction of flow with moving free surface is very important. Various researches were carried out to simulate these flows. Hughes *et al.* [1] solved the Navier–Stokes equations using the penalty function formulation. Bathe *et al.* [2] have

*Correspondence to: Yong-Taek Im, Computer Aided Materials Processing Laboratory, Department of Mechanical Engineering, ME3227, Korea Advanced Institute of Science and Technology, 373-1 Gusongdong, Yusonggu, Taejon 305-701, South Korea.
†E-mail: ytim@kaist.ac.kr
‡E-mail: sslee@kaist.ac.kr

Received 24 January 2004
Revised 27 August 2004
Accepted 15 December 2004

developed the ADINA-F finite element programme for fluid flow analysis with free surfaces and structural interactions.

The flow simulations with free surfaces can be based on either a moving mesh or a fixed mesh strategy. In the first case, called the Lagrangian method, only the fluid domain is meshed and the location of the fluid front is represented by a set of deformed meshes. In the second one, called the Eulerian method, the mesh is fixed and the free surface moves through it. Although the first strategy seems quite natural since the boundary of the fluid domain can be well known, it is limited by the mesh distortion and the contact treatment. The Lagrangian method can be improved by using an arbitrary Lagrangian–Eulerian method [3–7]. However, in complex three-dimensional flow, it is very difficult to determine how to move the boundary meshes. Therefore, the Eulerian method was adopted for numerical simulations in this study. In this approach, the numerical technique must be coupled with a technique to track the advecting fluid boundaries and interfaces.

Front-tracking techniques are divided into two groups: surface- and volume-tracking methods. In the surface-tracking methods, markers are initially located on the interface and are subsequently followed within the flow. These techniques give an accurate description of the free surface. However, interfacial mechanisms such as coalescence cannot be easily treated with these techniques. Moreover, for large and complex motion, the marker points will be non-uniformly distributed causing numerical instability as the interface evolves.

In the volume-tracking methods, the interface is implicitly tracked. Here, knowing the initial interface location and the velocity field, the surface is advected using the volume fraction field and reconstructed based on the newly calculated volume fractions. The interface is located somewhere in partially filled cells. The two commonly used methods are the volume of fluid (VOF) [8–15] and pseudo-concentration methods [16–19]. The VOF technique defines a marker function F, which represents the fraction of a cell volume occupied by one of the fluids. For a given cell, if F is zero or unity, the cell is considered to be either empty or filled with the fluid, respectively. If F is a value between zero and unity, the cell is an interface cell. The pseudo-concentration method is an extension of the volume tracking approach based on a marker function to finite element unstructured meshes. In this technique, a marker function, named pseudo-concentration, was designed to be advected by a standard finite element computation. The main feature of this function is that it is continuous on the whole domain and therefore can be accurately represented by finite element interpolation.

The advantage of these volume tracking methods is that they can handle the most complex free surface flow problems. Surface breaking and merging can be treated with this technique. However, these techniques have a major shortcoming. Although the interface itself can be located inside a cell, the governing equations for the field variables are applied for the whole cell. This results in significant inaccuracies in the treatment of the interface viscous stresses and the surface tension forces. To overcome these shortcomings, mesh fitting by dividing those cells crossed by the flow front interface into several cells was developed. This approach has been used by Sato and Richardson [20] and Mashayek and Ashgriz [21] for structured finite volume meshes and by Lock *et al.* [22] for fully unstructured triangular finite element meshes. However, all the proposed techniques are limited to two-dimensional cases so far. In the present study, the fringe element reconstruction method for general tetrahedral finite element mesh was developed. Here, the flow front was advected in a Lagrangian way, and new elements were constructed as a part of the original mesh where the fluid exists. Therefore, this method is able to accurately describe material discontinuity across the interface for

three-dimensional flow and can also take into account an interfacial phenomenon such as surface tension.

GOVERNING EQUATIONS

In this study, a mixed formulation of the governing flow equations was used to compute the flow field. The momentum and mass conservations of a Newtonian fluid flow are described by the Navier–Stokes equations:

$$\rho\left(\frac{\partial v_i}{\partial t}+v_{i,j}v_j\right)=\{-p\delta_{ij}+\mu(v_{i,j}+v_{j,i})\},j+f_i^{\mathrm{B}} \quad \text{on } \Omega \tag{1}$$

$$v_{i,i}=0 \quad \text{on } \Omega \tag{2}$$

where t, ρ, v_i, p, and μ denote the time, density, velocity in the x_i direction, pressure, and viscosity in that order, and f_i^{B} is the body force.

Typically, the following boundary conditions are imposed:

$$v_i=v_i^* \quad \text{on } S_u, \text{ (the Dirichlet boundary condition)} \tag{3}$$

$$t_i=t_i^* \quad \text{on } S_f, \text{ (the Neumann boundary condition)} \tag{4}$$

where v_i^* and t_i^* denote the prescribed velocity and traction. S_u and S_f are the parts of the boundary with Dirichlet and Neumann boundary conditions, respectively.

On the free surface, the effect of surface tension must be considered. In this study, it was assumed that the surface tension is constant along the free surface. Thus, the Neumann boundary condition on the free surface can be represented as follows:

$$\delta t_i=\sigma\left(\frac{1}{R_1}+\frac{1}{R_2}\right)n_i \quad \text{on the free surface} \tag{5}$$

where σ is the surface tension coefficient, R_1 and R_2 are the principal radii of curvature, respectively, and n_i is the direction cosine of the unit normal to the outer surface.

FINITE ELEMENT FORMULATION

A Galerkin-type weighting function was used here. The weighting functions for the velocity vector and pressure scalar are denoted as $\bar{\mathbf{v}}$ and $\bar{p}$, respectively, and the final weak form after the integration by parts can be written as follows:

$$\int_V \rho\frac{\partial v_i}{\partial t}\bar{v}_i\,\mathrm{d}V+\int_V \rho v_j v_{i,j}\bar{v}_i\,\mathrm{d}V-\int_V p\bar{v}_{i,i}\,\mathrm{d}V+\int_V(\mu v_{i,j}+\mu v_{j,i})\bar{v}_{i,j}\,\mathrm{d}V$$
$$=\int_V f_i\bar{v}_i\,\mathrm{d}V+\int_{S_f}t_i^*\bar{v}_i\,\mathrm{d}S \tag{6}$$

$$\int_V \bar{p} v_{i,i} \, \mathrm{d}V = 0 \tag{7}$$

A mixed finite element formulation based on four-node tetrahedral P1+/P1 elements has been implemented in this work. This element having the fifth node in its centroid satisfies the Babuska–Brezzi conditions [23], which are necessary to ensure a stable solution for the Navier–Stokes equations using the classical Galerkin method. In addition, it represents several important advantages: (1) the four-node element provides a minimum dimension of the element matrix compared with other three-dimensional finite elements; and (2) tetrahedral elements have a great ability to represent the complex geometries.

The trial function for velocity is constituted by four linear components and a bubble function. The pressure is defined linearly using the four vertices. In this work, a bubble function has zero at the element boundary and 1 at the centroid.

$$\mathbf{v} = \sum_{i=1}^{4} N_i \mathbf{v}_i + N_\mathrm{b} \mathbf{v}_\mathrm{b} = \sum_{\beta=1}^{5} N_\beta \mathbf{v}_\beta, \quad N_\mathrm{b} = \begin{cases} 0 & \text{at vertices} \\ 1 & \text{at centroid} \end{cases} \tag{8}$$

$$p = \sum_{i=1}^{4} N_i p_i = \sum_{\gamma=1}^{4} \tilde{N}_\gamma p_\gamma \tag{9}$$

where $\mathbf{v}$ and $\mathbf{v}_\mathrm{b}$ are velocity vectors at the vertices and the centroid, respectively. p_i is the pressure at the vertices, N_i the component of the linear trial functions and N_b the bubble function.

Even though the centroid is used as a part of the velocity field approximation when building the elementary matrices, it can then be eliminated by the 'static condensation' procedure at the element level, leading to the initial four-node tetrahedrons.

The finite element discretization of the flow equations leads to a highly non-linear system.

$$\mathbf{M}\dot{\mathbf{v}} + \mathbf{C}\mathbf{v} + \mathbf{N}(\mathbf{v}) = \mathbf{F} \tag{10}$$

$$\mathbf{M} = \begin{bmatrix} \displaystyle\int_V \rho \delta_{ij} N_\alpha N_\beta \, \mathrm{d}V & 0 \\ 0 & 0 \end{bmatrix} \tag{11}$$

$$\mathbf{C} = \begin{bmatrix} \displaystyle\int_V \mu (N_{\alpha,j} N_{\beta,i} + \delta_{ij} N_{\alpha,k} N_{\beta,k}) \, \mathrm{d}V & \displaystyle\int_V N_{\alpha,i} \tilde{N}_\gamma \, \mathrm{d}V \\ \displaystyle\int_V N_{\beta,i} \tilde{N}_\delta \, \mathrm{d}V & 0 \end{bmatrix} \tag{12}$$

$$\mathbf{N}(\mathbf{v}) = \begin{bmatrix} \displaystyle\int_V \rho \delta_{ij} N_\alpha N_{\beta,k} v_k \, \mathrm{d}V & 0 \\ 0 & 0 \end{bmatrix} \tag{13}$$

$$\mathbf{F} = \begin{Bmatrix} \int_V f_i N_\alpha \, \mathrm{d}V + \int_{S_f} t_i^* N_\alpha \, \mathrm{d}S \\ 0 \end{Bmatrix} \tag{14}$$

$$\mathbf{v} = \begin{Bmatrix} v_{j\beta} \\ p_\gamma \end{Bmatrix} \tag{15}$$

The predictor–corrector methods were implemented to solve the nonlinear equations and summarized as follows:

$$(\mathbf{M} + \gamma \Delta t \mathbf{C}) \tilde{\mathbf{v}}_{n+1}^{(i+1)} = \mathbf{M} \tilde{\mathbf{v}}_{n+1} + \gamma \Delta t \lfloor \mathbf{F}_{n+1} - N(\mathbf{v}_{n+1}^{(i)}) \rfloor \quad \text{(corrector)} \tag{16}$$

$$\tilde{\mathbf{v}}_{n+1} = \mathbf{v}_n + (1-\gamma)\Delta t \mathbf{a}_n \quad \text{(predictor)} \tag{17}$$

$$\mathbf{v}_{n+1}^{(0)} = \tilde{\mathbf{v}}_{n+1} \tag{18}$$

$$\mathbf{a}_{n+1} = (\mathbf{v}_{n+1} - \tilde{\mathbf{v}}_{n+1})/(\gamma \Delta t) \tag{19}$$

where Δt is the time step; $\mathbf{F}_n = \mathbf{F}(t_n)$; $\mathbf{v}_n$ and $\mathbf{a}_n$ are the approximations of $\mathbf{v}(t_n)$ and $\dot{\mathbf{v}}(t_n)$, respectively; γ is a positive parameter that governs the stability and accuracy of the algorithm; and superscripts in parentheses are iteration numbers. If I denotes the total number of iterations to be performed, then the velocity at time t_{n+1} is defined by

$$\mathbf{v}_{n+1} = \mathbf{v}_{n+1}^{(I+1)} \tag{20}$$

Given $\mathbf{v}_n$ and $\mathbf{a}_n$, (16)–(20) serve to uniquely define $\mathbf{v}_{n+1}$ and $\mathbf{a}_{n+1}$.

FRINGE ELEMENT RECONSTRUCTION

In an Eulerian description of moving interface flows, the flow front generally does not coincide with element faces. To overcome this drawback, a local and temporary mesh fitting scheme, made by dividing elements at the flow front interface into several elements, was developed by Sato and Richardson [20], Mashayek and Ashgriz [21], and Lock *et al.* [22]. To extend these methods to three-dimensional flow, the fringe element reconstruction method for general tetrahedral finite element mesh was developed in this study. This method was composed of several steps as shown in Figure 1. Details of each step are as follows:

Tracing the free surface

The basic idea of the front tracking method is fairly simple. At first, the initial boundary surface was given with triangular elements. Then, the boundary surface was advected by the Lagrangian method as

$$\mathbf{x}_{n+1} = \mathbf{x}_n + \Delta t \mathbf{v}_n \tag{21}$$

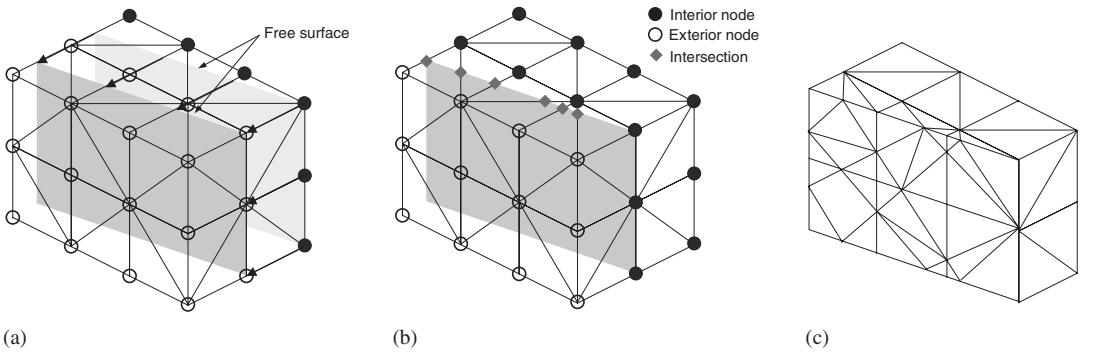

Figure 1. Illustration of the front tracking and fringe element reconstruction method: (a) tracing the free surface; (b) determining the position of the intersection between the free surface and element edges; and (c) reconstruction of fringe element.

where $\mathbf{x}_n$ is the position of the boundary surface at time step n and $\mathbf{v}_n$ is the velocity at position $\mathbf{x}_n$. From this process, the boundary surface at the next time step can be constructed.

Determining intersection points and reconstructing fringe elements

To reconstruct the fringe elements, the precise position of the intersection between the free surface and element edges must be determined. At each time step, each node has a flag that indicates whether it is inside the fluid or not. If all nodes have flags of unity, this element is assumed to be filled with fluid. If all nodes have flags of zero, the element is empty. The free surface is located within elements that are composed of nodes that have both unity and zero flags. When the free surface penetrates the original mesh system, the intersection points between the free surface and element edges become new nodes for the fringe elements. Because the intersection points exist in the edges that have different nodal flags, 0 and 1, the position of the free surface can be roughly known. The precise position of the intersection can then be determined by finding directly the intersection points between these edges and the triangle elements that construct the free surface.

Each element in which the free surface exists was reconstructed into several tetrahedral elements according to its filling state. Figure 2 shows seven types of fringe elements reconstructed in an original element. In reconstructing fringe elements, caution must be taken not to generate two contacting faces that are inconsistent, as shown in Figure 3.

Occasionally, extremely small fringe elements are generated. This situation is encountered when the free surface intersects an element edge very close to one of its vertex nodes. It possibly deteriorates the speed of computation because of a Courant–Friedrichs–Lewy (CFL) stability condition [24]. To overcome this difficulty, a cutting-out criterion has been introduced. If a certain edge of the fringe element crosses over the flow front, the distance D between the intersection point and the nearest vertex node is compared with the length L of the penetrating edge. Then a new node is generated at the intersection point only if the following condition is satisfied:

$$D \geqslant \varepsilon L, \quad (0 < \varepsilon \ll 1) \tag{22}$$

Number of interior nodes	Number of intersection points	Filling state	Element reconstruction
1	3	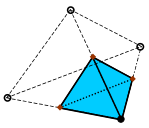	
2	4	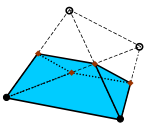	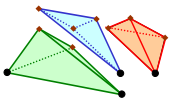
	3	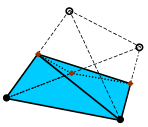	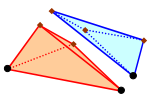
	2	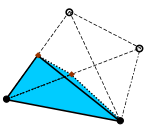	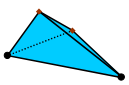
3	3	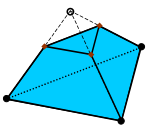	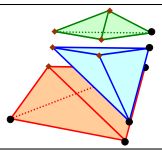
	2	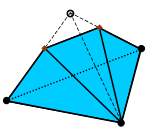	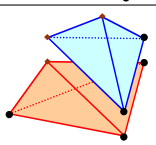
	1	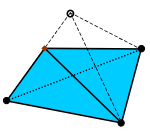	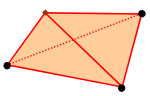

Figure 2. Seven cases of mesh reconstruction in the front elements.

The magnitude of ε was chosen to be 0.05 in this study. When this condition was not satisfied, the nearest vertex node was moved to the free surface as shown in Figure 4. As a result, extremely small fringe elements disappeared.

Extrapolation of velocity

At the beginning of each time step of computation, newly filled nodes do not have velocities yet. Here, front-tracking arbitrary Lagrangian–Eulerian (FTALE) formulation [7] was used

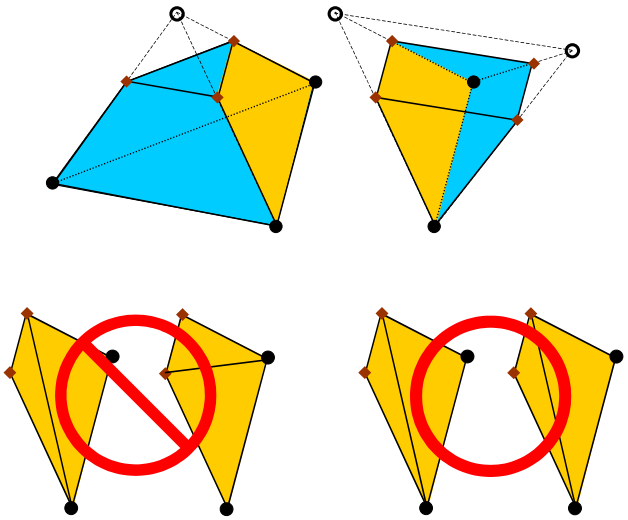

Figure 3. Two contacting faces of: (a) wrong case; and (b) correct case.

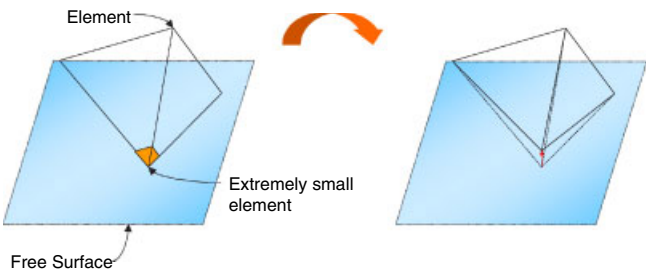

Figure 4. Exclusion of extremely small element by moving node.

for obtaining velocities at such nodes. Figure 5 shows the situation of an interface travelling from left to right. The numerical approximation of the time derivative $\partial v/\partial t$ at time $t+\Delta t$ for a node that encountered an interface at time $t+\alpha\Delta t$, with $0<\alpha<1$, was obtained as follows.

Let $x^I(t)$ designate the location of the interface at time t, and let the interface encounter the node located at point x at time $t+\alpha\Delta t$. At time t, $v^-(x^I(t),t)$ and $v^+(x^I(t),t)$ are the left and right values of v at the interface, respectively. Here, the notation of left and right values is related to the orientation of the unit normal vector $\mathbf{n}$ to the interface. The time rate of change $\partial v/\partial t$ at the interface can be represented by

$$\left(\frac{\partial v}{\partial t}\right)_{(x,t+\Delta t)} = \frac{v(x,t+\Delta t)-v^-(x,t+\alpha\Delta t)}{(1-\alpha)\Delta t} \tag{23}$$

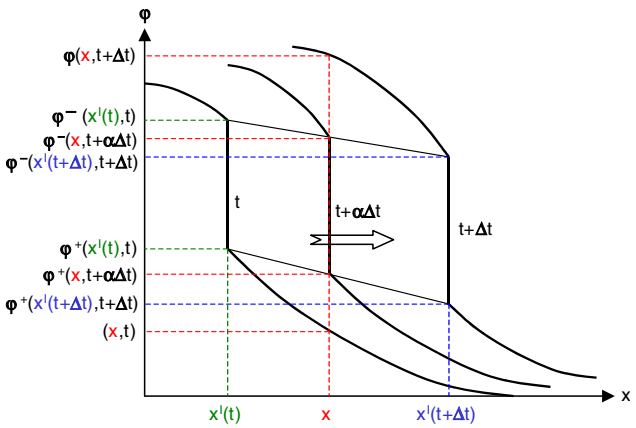

Figure 5. One-dimensional representation of the jump of a scalar field φ near the interface travelling from left to right in the time interval $[t, t+\Delta t]$.

This can be approximated as

$$\left(\frac{\partial v}{\partial t}\right)_{(x,t+\Delta t)} \approx \frac{v(x,t+\Delta t) - v^{-}(x^{I}(t),t)}{\Delta t} - \left(\frac{x - x^{I}(t)}{\Delta t}\right)\left(\frac{\partial v}{\partial x}\right)_{(x,t+\Delta t)} \tag{24}$$

The extension to the multi-dimensional case can be easily made as

$$\left(\frac{\partial \mathbf{v}}{\partial t}\right)_{(\mathbf{x},t+\Delta t)} \approx \frac{\mathbf{v}(\mathbf{x},t+\Delta t) - \mathbf{v}^{-}(\mathbf{x}^{I}(t),t)}{\Delta t} - \left(\frac{\mathbf{x} - \mathbf{x}^{I}(t)}{\Delta t}\right) \cdot (\operatorname{grad} \mathbf{v})_{(\mathbf{x},t+\Delta t)} \tag{25}$$

This equation can be transformed as

$$\left(\frac{\partial \mathbf{v}}{\partial t}\right)_{(\mathbf{x},t+\Delta t)} \approx \frac{\mathbf{v}(\mathbf{x},t+\Delta t) - \{\mathbf{v}^{-}(\mathbf{x}^{I}(t),t) + (\mathbf{x} - \mathbf{x}^{I}(t)) \cdot (\operatorname{grad} \mathbf{v})_{(\mathbf{x},t+\Delta t)}\}}{\Delta t} \tag{26}$$

And the velocities of newly filled nodes can be approximated as

$$\begin{aligned} \mathbf{v}_{(\mathbf{x},t)} &\approx \mathbf{v}^{-}(\mathbf{x}^{I}(t),t) + (\mathbf{x} - \mathbf{x}^{I}(t)) \cdot (\operatorname{grad} \mathbf{v})_{(\mathbf{x},t+\Delta t)} \\ &\approx \mathbf{v}^{-}(\mathbf{x}^{I}(t),t) + (\mathbf{x} - \mathbf{x}^{I}(t)) \cdot (\operatorname{grad} \mathbf{v})_{(\mathbf{x},t)} \end{aligned} \tag{27}$$

Surface tension modelling

In Equation (5), the surface tension force was modelled with the unit normal vector and the principal radii of curvature at the free surface as shown in Figure 6(a). However, the calculation of the principal radii of curvature is not easy. Therefore, instead of finding the curvature, which involves higher order derivatives and whose calculation is in general not

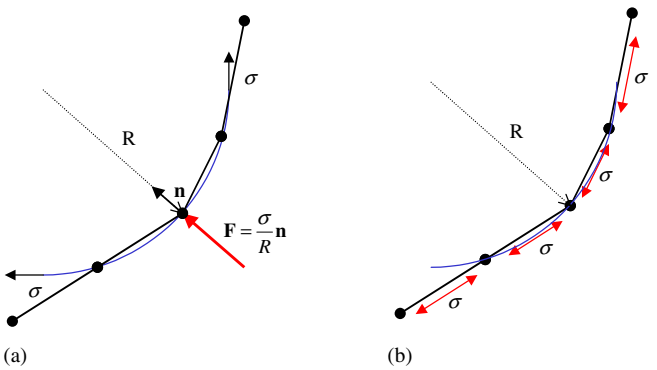

Figure 6. Schematic diagram of the method considering surface tension by means of: (a) resultant surface force; and (b) surface tension.

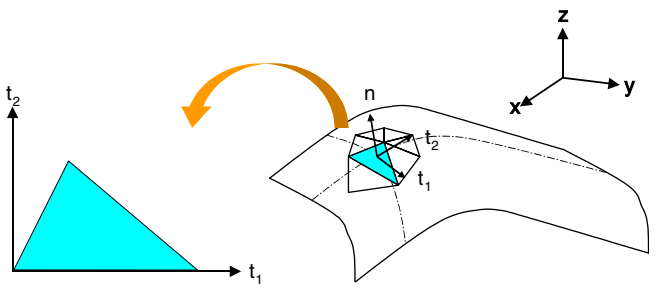

Figure 7. Schematic diagram of the triangular element on the free surface.

accurate, the boundary condition for surface tension was directly satisfied on the free surface as shown in Figure 6(b). It was accomplished by attaching triangle elements that had tensile residual stress σ. The force on each surface triangle element was determined as

$$f_k = \int_{S_{\text{tri}}} (\sigma)_{kl} N_{\alpha,l} \, \mathrm{d}s \tag{28}$$

Here, k and l are notations denoting the tangent direction t_1 and t_2 as shown in Figure 7, and N_α is the shape function of the triangle element. The force vector can be transformed to the global co-ordinate as follows:

$$\begin{Bmatrix} f_{t_1} \\ f_{t_2} \\ f_n \end{Bmatrix} = \mathbf{T} \begin{Bmatrix} f_x \\ f_y \\ f_z \end{Bmatrix} \tag{29}$$

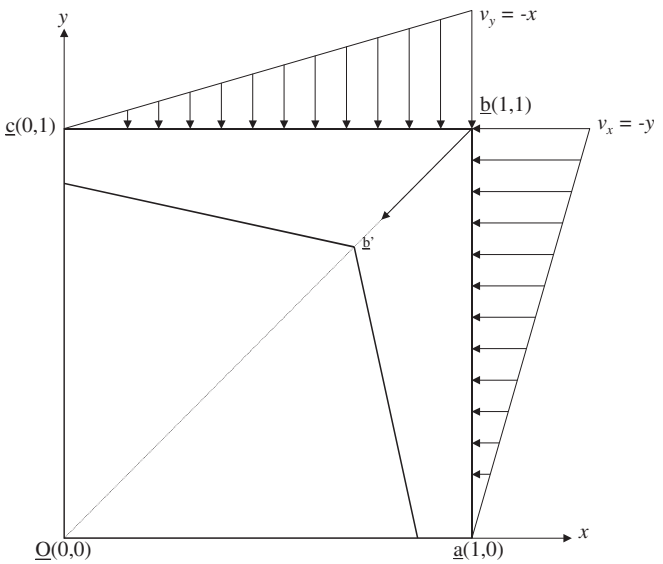

Figure 8. Schematic diagram of a given velocity field problem.

$$\mathbf{T} = \begin{bmatrix} \mathbf{t}_1 \\ \mathbf{t}_2 \\ \mathbf{n} \end{bmatrix}, \quad \mathbf{t}_1 \cdot \mathbf{t}_2 = \mathbf{0}, \quad \mathbf{t}_1 \times \mathbf{t}_2 = \mathbf{n} \tag{30}$$

The transformed force is then applied to the nodes on the free surface. This method ensures that the total force on any closed surface is zero since the forces on each edge of every triangle element exactly cancel each other. This conservative property is particularly important for long-time computation where even a small error in the surface tension computation can lead to an unphysical net force on the interface that can be accumulated over time.

NUMERICAL EXAMPLES

In order to verify the numerical results obtained from the developed programme, some numerical examples are presented in the following.

Analytical case

The example as shown in Figure 8 is a unit square where a velocity field was imposed as in Reference [25]

$$v_x = -y, \quad v_y = -x \tag{31}$$

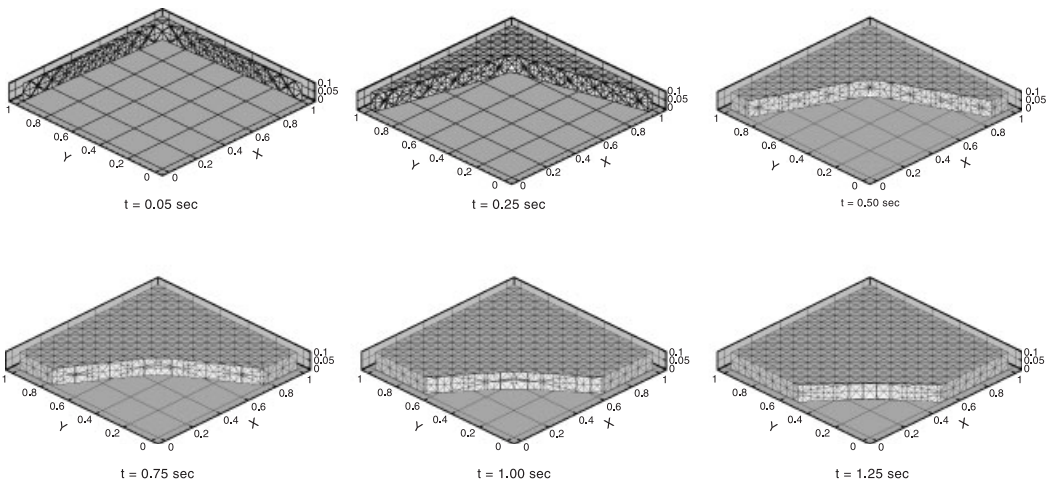

Figure 9. Flow front positions and corresponding mesh structure.

Since the velocity (31) is steady, the particle pathlines and the streamlines are coincident, and governed by

$$y^2 = x^2 + c \tag{32}$$

where c is a constant.

The magnitude of the velocity $|v|$ is equal to $(x^2 + y^2)^{1/2}$. As the fluid fills the square cavity from the top and right sides, the velocity diminishes and vanishes at the origin $\underline{o}$. The analytical solution of the non-dimensional displacement (d/D) versus the filling time can be obtained as follows:

$$d/D = 1 - \mathrm{e}^{-t} \tag{33}$$

where d is the particle displacement $|\underline{bb'}|$ and D is the length of the diagonal $|\underline{bo}|$.

Flow fronts and corresponding reconstructed mesh structure are shown in Figure 9. In order to compare with the analytical solution, the flow front position at the diagonal was collected at various times as shown in Figure 10. A very good agreement between the numerical prediction and analytical solution was obtained during the entire filling process.

Broken dam problem

A column of water in hydrostatic equilibrium was initially confined between two vertical walls as shown in Figure 11. At initial time ($t = 0$), the right wall was suddenly removed and the water column flowed out under gravity along a dry horizontal floor. The water column was chosen to be $a = 5.715$ cm wide and $b = 11.430$ cm high in order to compare this numerical solution with the experimental data obtained by Martin and Moyce [26]. The density and the dynamic viscosity were 1000 kg/m^3 and 0.001 kg/ms, respectively. No surface tension force was applied since its effect was negligible compared with the gravity force. The boundary conditions used in the calculation are indicated in Figure 11.

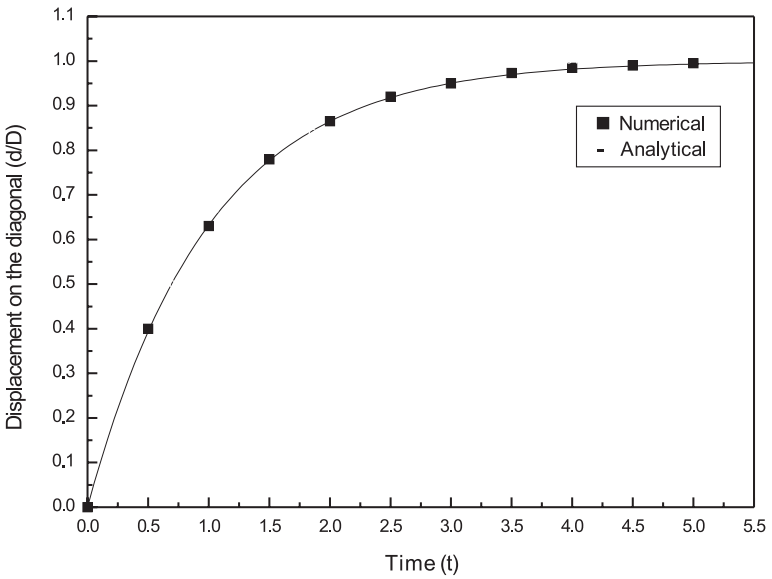

Figure 10. Comparison of the numerical prediction with the analytical solution [25].

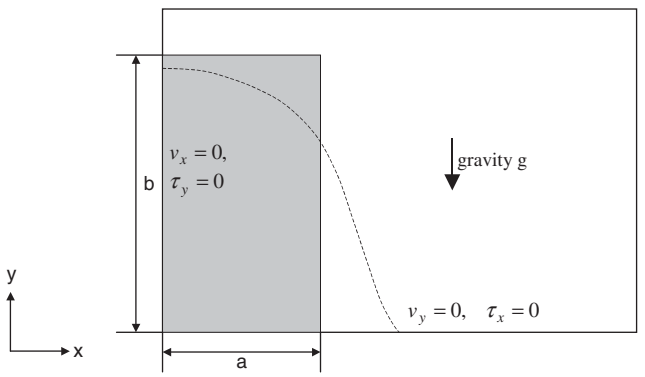

Figure 11. Schematic diagram for the broken dam problem.

The predicted water front location along the floor has been compared with Martin and Moyce's experimental data. For comparison of numerical solutions with the experimental results, dimensionless time and water front location along the bottom were defined as $t^* = t\sqrt{2g/a}$ and $z^* = z/a$, respectively. As shown in Figure 12, calculation results show good agreement with the experimental data.

Filling simulation of a crank shaft part

Filling analysis of a crank shaft part was also performed using the current model. The geometry and the dimension used in simulations are shown in Figure 13. Only half of the geometry was

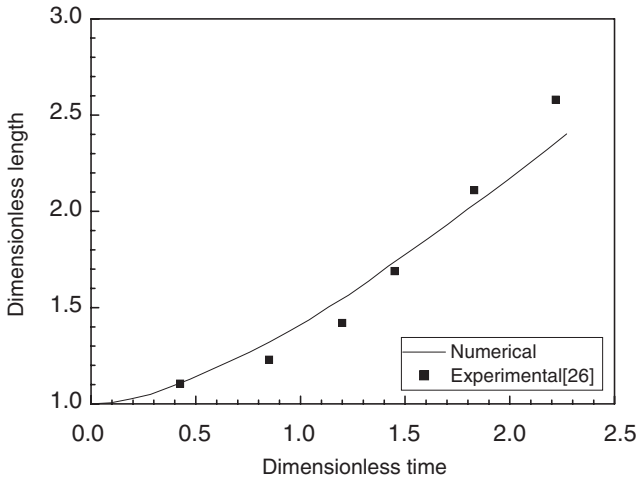

Figure 12. Water front location $z^* = z/a$ versus time $t^* = t\sqrt{2g/a}$ along the floor.

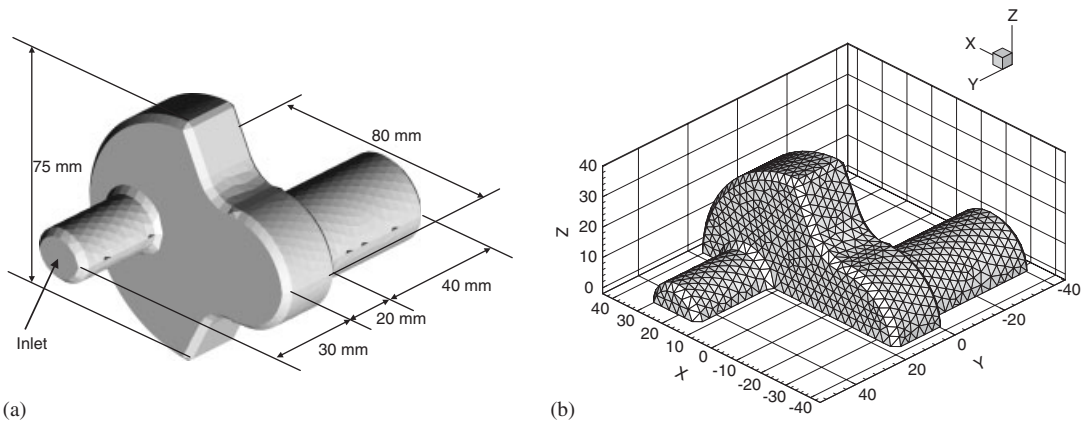

Figure 13. (a) Geometry of the crank shaft part; and (b) its mesh layout.

meshed using tetrahedral elements. The mesh used for the filling analysis consists of 3751 nodes and 18 003 elements. The density and viscosity were assumed to be 0.81 kg/mm^3 and 3.6 kg/mm s, respectively. No slip condition was applied at all surfaces of the cavity and the inlet velocity was 600 mm/s.

The flow front positions and corresponding velocity magnitudes are represented in Figure 14 at different filling times. It shows that a boundary layer was formed near the surface due to the no slip condition, resulting in lower velocity at the surface and higher velocity in the core. However, the velocities in the core became lower at the free surface region because the flow began to spread out. This model simulation result confirmed that the currently developed programme can adequately analyse three-dimensional moving free surface problems.

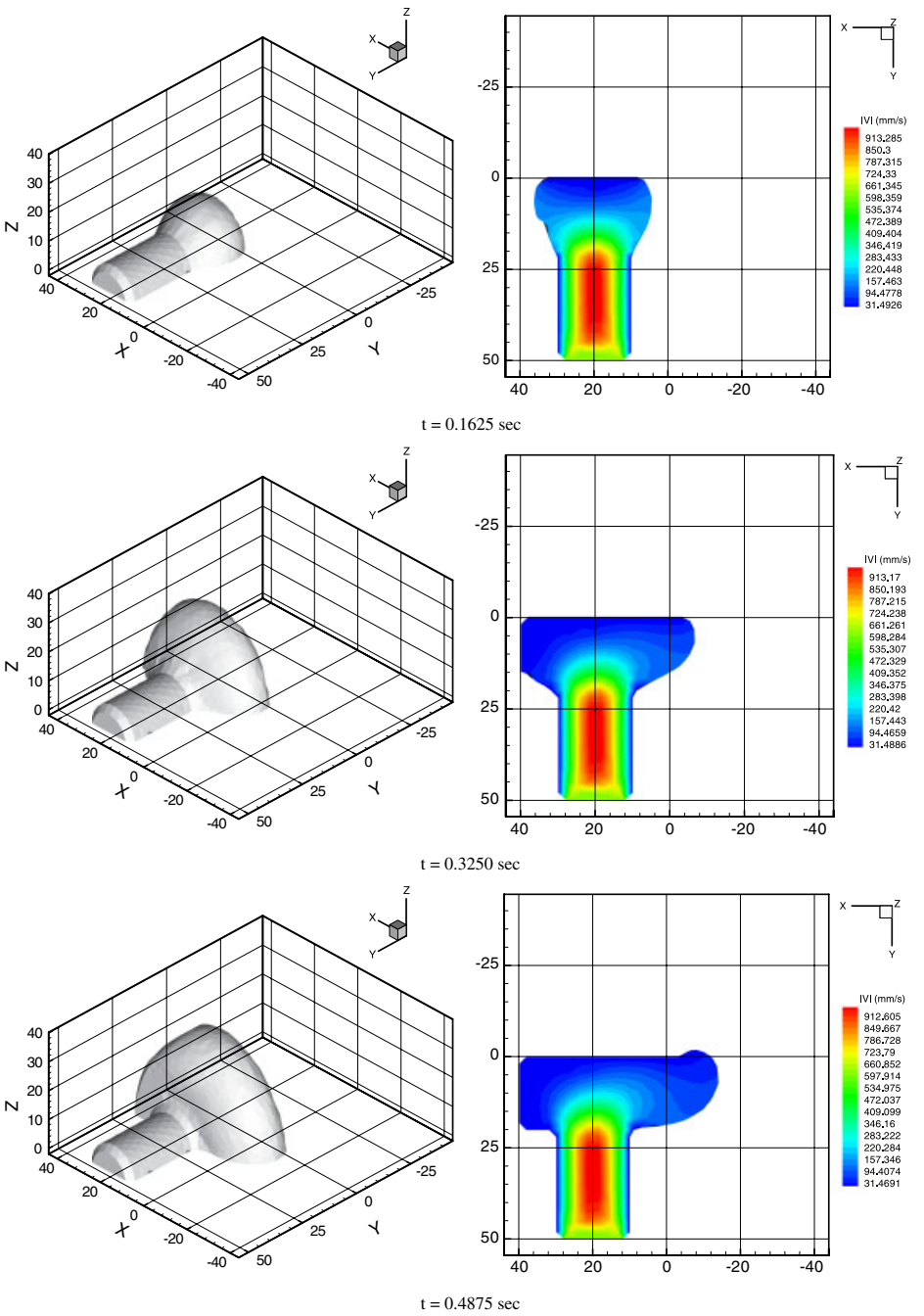

Figure 14. Flow front positions and corresponding velocity magnitudes $|v|$ at the six filling stages of the crank shaft part.

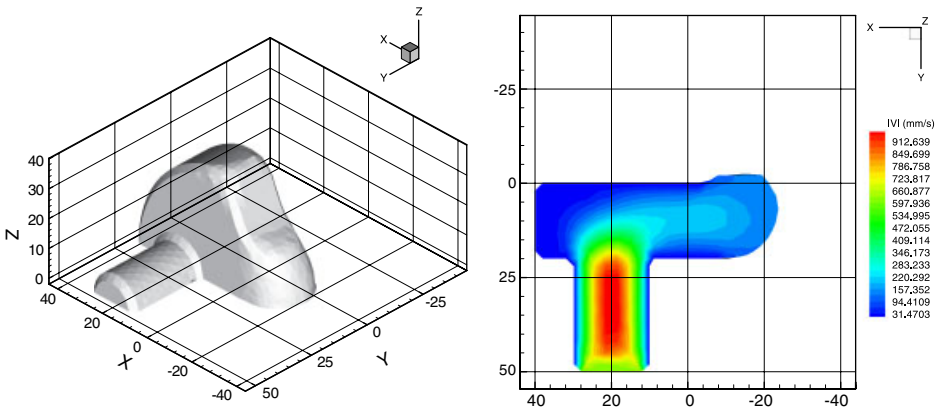

t = 0.6500 sec

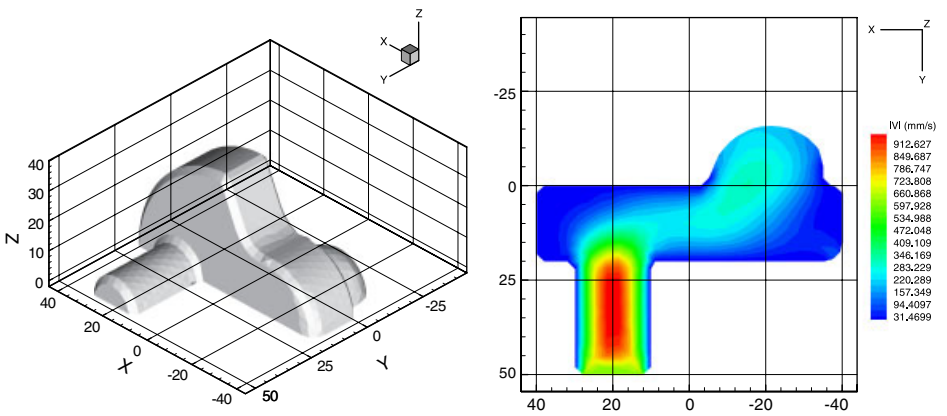

t = 0.8125 sec

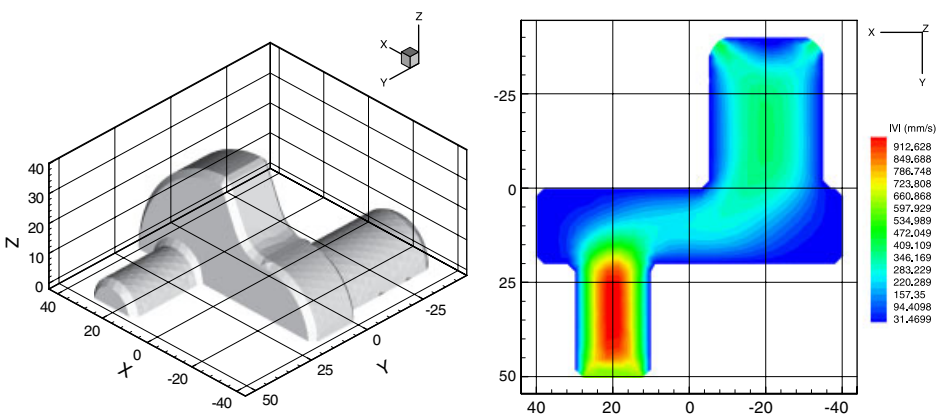

t = 0.9620 sec

Figure 14. *Continued*

CONCLUSIONS

A front tracking and fringe element reconstruction method has been developed to simulate three-dimensional incompressible flow with moving free surface. To solve the Navier–Stokes equations, a mixed formulation based on a four-node tetrahedral element with a bubble function at the centroid (P1+/P1) was employed. In order to keep material discontinuity across the interface accurate, the element penetrated by the free surface was divided and reconstructed along the flow front. This method provides more accurate results, because the element faces coincide with the flow front interface, and also leads to improved treatment of boundary conditions for the free surface in the finite element formulation. The surface tension effect was considered by imposing the tensile stress on surface elements. This method requires no calculation of the surface curvature and ensures conservation of the total surface force. The accuracy of the developed programme was verified by comparing the results to the exact solution and experimental data in the literature. Also, a filling problem of a crank shaft was analysed in order to demonstrate the efficiency of the proposed method. It was found that the currently developed method was useful in the three-dimensional analysis of free surface moving problems.

REFERENCES

1. Hughes TJR, Liu WK, Brooks A. Finite element analysis of incompressible viscous flows by the penalty function formulation. *Journal of Computational Physics* 1979; **30**:1–60.
2. Bathe KJ, Zhang H, Wang MH. Finite element analysis of incompressible and compressible fluid flows with free surfaces and structural interactions. *Computers and Structures* 1995; **56**:193–213.
3. Hirt CW, Amsden AA, Cook JL. An arbitrary Lagrangian–Eulerian computing method for all flow speeds. *Journal of Computational Physics* 1974; **14**:227–253.
4. Hughes TJ, Liu WK, Zimmermann TK. Lagrangian–Eulerian finite element formulation for incompressible viscous flows. *Computer Methods in Applied Mechanics and Engineering* 1981; **29**:329–349.
5. Belytschko T, Flanagan DP, Kennedy JM. Finite element methods with user-controlled meshes for fluid–structure interaction. *Computer Methods in Applied Mechanics and Engineering* 1982; **33**:669–688.
6. Donea J, Giuliani S, Halleux JP. An arbitrary Lagrangian–Eulerian finite element methods for transient dynamic fluid–structure interactions. *Computer Methods in Applied Mechanics and Engineering* 1982; **33**:689–723.
7. Jaeger M, Carin M. The front-tracking ALE method: application to a model of the freezing of cell suspensions. *Journal of Computational Physics* 2002; **179**:704–735.
8. Nichols BD, Hirt CW, Hotchkiss RS. SOLA-VOF: a solution algorithm for transient fluid flow with multiple free boundaries. *Technical Report LA-8355*, Los Alamos Scientific Laboratory, 1980.
9. Hirt CW, Nichols BD. Volume of fluid (VOF) method for the dynamics of free boundaries. *Journal of Computational Physics* 1981; **39**:201–225.
10. Rider WJ, Kothe DB. Reconstructing volume tracking. *Journal of Computational Physics* 1998; **141**:112–152.
11. Shin S, Lee WI. Finite element analysis of incompressible viscous flow with moving free surface by selective volume of fluid method. *International Journal of Heat and Fluid Flow* 2000; **21**:197–206.
12. Černe G, Petelin S, Tiselj I. Numerical errors of the volume-of-fluid interface tracking algorithm. *International Journal for Numerical Methods in Fluids* 2002; **38**:329–350.
13. Černe G, Petelin S, Tiselj I. Coupling of the interface tracking and the two-fluid models for the simulation of incompressible two-phase flow. *Journal of Computational Physics* 2001; **171**:776–804.
14. Renardy M, Renardy Y, Li J. Numerical simulation of moving contact line problems using a volume-of-fluid method. *Journal of Computational Physics* 2001; **171**:243–263.
15. Chen L, Li Y. A numerical method for two-phase flows with an interface. *Environmental Modelling & Software* 1998; **3**:247–255.
16. Thompson E. Use of pseudo-concentrations to follow creeping viscous flows during transient analysis. *International Journal for Numerical Methods in Fluids* 1986; **6**:749–761.
17. Haagh GAAV, Van de Vosse FN. Simulation of three-dimensional polymer mould filling processes using a pseudo-concentration method. *International Journal for Numerical Methods in Fluids* 1998; **28**:1335–1369.
18. Wang SP, Wang KK. A net inflow method for incompressible viscous flow with moving free surface. *International Journal for Numerical Methods in Fluids* 1994; **18**:669–694.

19. Medale M, Jaeger M. Numerical simulation of incompressible flows with moving interfaces. *International Journal for Numerical Methods in Fluids* 1997; **24**:615–638.
20. Sato T, Richardson SM. Numerical simulation method for viscoelastic flows with free surfaces—fringe element generation method. *International Journal for Numerical Methods in Fluids* 1994; **19**:555–574.
21. Mashayek F, Ashgriz N. A hybrid finite-element-volume-of-fluid method for simulating free surface flows and interfaces. *International Journal for Numerical Methods in Fluids* 1995; **20**:1363–1380.
22. Lock N, Jaeger M, Medale M, Occelli R. Local mesh adaptation technique for front tracking problems. *International Journal for Numerical Methods in Fluids* 1998; **28**:719–736.
23. Brezzi F, Bathe KJ. A discourse on the stability conditions for mixed finite element formulation. *Computer Methods in Applied Mechanics and Engineering* 1990; **82**:27–57.
24. Courant R, Friedrichs K, Lewy H. Über die Partiellen Differenzengleichungen der Mathematischen Physik. *Mathematische Annalen* 1928; **100**:32–74.
25. Gao DM. A three-dimensional hybrid finite element-volume tracking model for mould filling in casting process. *International Journal for Numerical Methods in Fluids* 1999; **29**:877–895.
26. Martin JC, Mocye WJ. An experimental study of the collapse of liquid columns on a rigid horizontal plane. *Philosophical Transactions of the Royal Society of London Series A-Mathematical, Physical and Engineering Sciences* 1952; **244**:312–324.

